European Journal of Pharmaceutical Sciences 127 (2019) 330–338

Contents lists available at ScienceDirect

European Journal of Pharmaceutical Sciences

journal homepage: www.elsevier.com/locate/ejps

# Inclusion complexes of β-cyclodextrin and polymorphs of mebendazole: Physicochemical characterization

Elbio Saidman[a,1], Ana K. Chattah[b,1], Leslie Aragón[a], Matías Sancho[c], Gerardo Camí[d], Claudia Garnero[e,*], Marcela Longhi[e]

[a] Laboratorio de Control de Calidad de Medicamentos, Facultad de Química Bioquímica y Farmacia, Universidad Nacional de San Luis, Argentina
[b] Facultad de Matemática, Astronomía, Física y Computación, Universidad Nacional de Córdoba e IFEG, CONICET, Argentina
[c] Área de Química Física, Facultad de Química Bioquímica y Farmacia, Universidad Nacional de San Luis, IMIBIO, CONICET, Argentina
[d] Área de Química General e Inorgánica, Facultad de Química Bioquímica y Farmacia, Universidad Nacional de San Luis, Argentina
[e] Unidad de Investigación y Desarrollo en Ciencia y Tecnología Farmacéutica (UNITEFA-CONICET), Departamento de Ciencias Farmacéuticas, Facultad de Ciencias Químicas-Universidad Nacional de Córdoba, Ciudad Universitaria, X5000HUA Córdoba, Argentina

ARTICLE INFO

*Keywords:*
Mebendazole
Polymorph
Cyclodextrin
Complexes
Characterization
ssNMR

ABSTRACT

Mebendazole (MBZ), designated as a WHO essential drug, can exist in diverse solid forms and presents low absorption at the gastrointestinal level. Considering the potential of cyclodextrins to enhance the solubility and permeability of drugs, inclusion complexes of polymorphs A and C of MBZ with β-cyclodextrin were obtained. The characterization of the complexes in solid state was performed by using a combination of experimental techniques including Fourier transform infrared spectroscopy, powder X-ray diffractometry and solid state nuclear magnetic resonance. Moreover, the effect of the binary complexes on their physical stability was evaluated. In addition, for a complete characterization of polymorphs A and C, one dimensional spectra and correlation nuclear magnetic resonance experiments were employed. Our physical studies showed that the inclusion complexes were new crystalline forms that induced shifts and broadening in the infrared and nuclear spectra. A molecular modelling analysis performed on the inclusion modes, demonstrated that the most favourable structure for the complex was the head down orientation. Moreover, the intermolecular interactions calculated for the complex with the atoms in molecules theory are in good agreement with the spectroscopic results. The inclusion complexes exhibited an increment of solubility in simulated physiological media. Furthermore, it was demonstrated that the complex formation did not affect the physical stability of the polymorphs.

## 1. Introduction

Mebendazole (MBZ), designated as a WHO essential drug, is commonly used either in clinical or veterinary treatment as a broad spectrum anthelmintic drug. It is commercialized as a tablet formulation or as a suspension. This compound is efficiently applied in the treatment of infections produced by *Ascaris lumbricoides* (roundworm) and *Necator americanus* (hookworm) (Hollingsworth et al., 2015), or in other parasitic diseases, such as alveolar echinococcosis (Gottstein et al., 2016). In addition, MBZ has shown promising cytotoxic activity against a human malignant cell line derived from a primary gastric cancer tumour (Pinto et al., 2015). In particular, MBZ is especially recommended for the treatment of intestinal parasites in children, as previous studies have reported that the incidence of adverse side effects was negligible (Montresor et al., 2002, 2003). MBZ is practically insoluble in water (U.S. Pharmacopeia and the National Formulary, 2008) and therefore exhibits a poor absorption from the intestinal tract. There are three polymorphic forms of MBZ in the solid state (A, B and C), with different solubility and therapeutic effects. Their solubility in 0.1 M HCl is as follows: B (0.07 mg/mL) > C (0.04 mg/mL) > A (0.02 mg/mL). Several studies and clinical trials revealed that form A is not effective and form B is toxic; therefore, form C is pharmaceutically preferred and is, in fact, the form that registered products must contain (Chiba et al., 1991; Charoenlarp et al., 1993; Swanepoel et al., 2003).

Multiple techniques are currently utilized to improve the aqueous solubility of drugs, such as the salts formation, the formulation of amorphous phases, the use of microemulsions, liposomes and nanoparticles, and the formation of inclusion complexes with cyclodextrins

* Corresponding author.
*E-mail address:* garneroc@fcq.unc.edu.ar (C. Garnero).
[1] The authors contributed equally to the production of the article.

https://doi.org/10.1016/j.ejps.2018.11.012
Received 8 August 2018; Received in revised form 1 November 2018; Accepted 12 November 2018
Available online 13 November 2018
0928-0987/ © 2018 Published by Elsevier B.V.

(CDs) among others (Garnero et al., 2012; Aloisio et al., 2015; Surov et al., 2015; Martinez-Marcos et al., 2016). CDs are non-toxic, cyclic oligomers with a truncated cone shape that can be obtained from the biotransformation of starch (Jeang et al., 2005). The most common CDs are constituted by six, seven or eight units of α-(1 → 4)-D-glucose per molecule (α-, β- and γ-CD, respectively). The outer layer of the molecule is hydrophilic, and organic molecules with an appropriate size and shape, can be inserted into its hydrophobic cavity, forming non-covalent inclusion complexes as a result (Frömming and Szejtly, 1994). The inclusion process with CDs can increase the aqueous solubility of a drug, and also its general stability and bioavailability (Garnero et al., 2010; Zoppi et al., 2011; Meinguet et al., 2015; Mendes et al., 2016). In addition, β-CD is particularly useful as a pharmaceutical excipient, because of its cavity dimensions, low cost and higher production rates. The wide range of application of CDs in the pharmaceutical industry has generated numerous studies to elucidate the physicochemical and structural properties of the inclusion complexes between this polysaccharide and different drugs (Garnero et al., 2012; Chattah et al., 2013; De Oliveira et al., 2015; de Melo et al., 2016).

The anthelmintic efficacy of MBZ is highly dependent on its polymorphic nature. The C form is preferred for oral use, but it is metastable and may crystallize into the more stable A form, in the presence of high humidity and temperature. Moreover, the existence of small quantities of form A in tablets, results in a rapid increase of transformation. Unfortunately, form A is considered therapeutically ineffective. Considering the polymorphic nature of MBZ and the potential of β-CD to enhance its solubility, the purpose of this study was to obtain binary complexes of A and C polymorphs of MBZ and β-CD, and to investigate the interactions between the components in the solid state by experimental and theoretical analysis. The solid complexes were prepared by the freeze drying method. The interactions between the MBZ polymorphs and β-CD were analysed by using Fourier transform infrared spectroscopy (FT-IR), solid state nuclear magnetic resonance (ssNMR) and powder X-ray diffraction (PXRD). Moreover, an analysis by molecular modelling was performed to gain insights into the molecular geometry of the complex between MBZ and β-CD. By using the quantum theory of atoms in molecules (QTAIM) approximations, significant physicochemical interactions between the guest and host were analysed. Furthermore, taking into account that a solid state NMR evaluation of MBZ and its complexes with CDs has not been reported up to date, one dimensional (1D) and two dimensional (2D) ssNMR experiments were performed to provide an exhaustive characterization of MBZ polymorphs A and C, as well as to monitor the physical stability of the complexes. In addition, the solubility of the samples under study was evaluated.

## 2. Materials and methods

### 2.1. Reagents

Polymorphs A and C of MBZ (Fig. 1) were purchased from Androquímica SA (San Luis, Argentina). β-Cyclodextrin was kindly supplied by Ferromet agent in Argentina of Roquette (France). Double distilled water was purified using a Thermo Scientific Easypure II system, with conductivity lower than 1.8 μS $cm^{-1}$. All other chemicals were of analytical grade.

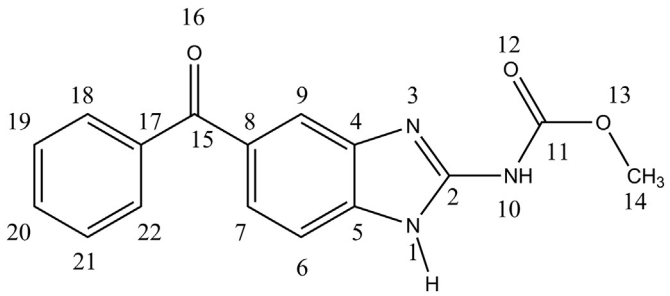


**Fig. 1.** Molecular structure of MBZ and the chemical numbering system adopted in this work.

### 2.2. Preparation of solid samples

Solid-state samples of MBZ A and C, in equimolar ratio with β-CD, were prepared as follows.

#### 2.2.1. Freeze drying (FD)

The binary complexes of MBZ, A and C (FD A and FD C, respectively), were prepared by mixing the reagents with an ethanol:water solution (80:20 v/v). The resulting suspension was sonicated at constant temperature (25.0 ± 0.1 °C) until the dissolution was complete. Then, ethanol was removed from the solution by rotary evaporation at 65 °C (Rotavapor Decalab. Argentina). The aqueous suspension was frozen at −40 °C for 24 h, and freeze-dried using a Rificor lyophiliser (model L-A-B5).

#### 2.2.2. Physical mixtures (PM)

The physical mixtures of MBZ, A and C (PM A and PM C, respectively), were prepared by adding the reagents into an agate mortar and uniformly grinding for 15 min at room temperature.

### 2.3. FT-IR

The FT-IR spectra of MBZ (A and C), β-CD and the solid binary samples were registered on a Shimadzu IR Affinity-1 DRS-800 spectrophotometer. The spectra were recorded in the 4000–400 $cm^{-1}$ interval, using the KBr pellet technique and with a spectral resolution of 2 $cm^{-1}$.

### 2.4. ssNMR

High resolution solid state $^{13}C$ spectra of MBZ (A and C), β-CD, the FDs (A and C) and the PMs (A and C) samples were recorded with the ramp cross polarization/magic angle spinning (CP-MAS) sequence, with proton decoupling during acquisition (Harris, 1986; Metz et al., 1994). All ssNMR experiments were performed at room temperature in a Bruker Avance II spectrometer, operating at 300.13 MHz for protons, which was equipped with a 4 mm MAS probe. The operating frequency for carbon was 75.46 MHz. Glycine was used as an external reference for the $^{13}C$ spectra and for setting the Hartmann–Hahn matching condition in the cross-polarization experiments. Spectra were recorded with 1600 scans, with the contact time during CP being 1.5 ms and the recycling times being 5 s in all cases. SPINAL-64 was used for proton decoupling during acquisition (Fung et al., 2000). The spinning rate for all the samples was 10 kHz. $^{13}C$ spectra, to study physical stability, were performed in the same conditions. Quaternary carbon and methyl groups-only spectra were also recorded for MBZ A and C, at 10 kHz MAS. Following the cross-polarization period, a delay of 40 μs was introduced prior to the acquisition without applying any radiofrequency pulses on $^{1}H$ and $^{13}C$ channels, resulting in a rapid decay for the CH and $CH_2$ signals, due to their strong $^{1}H$–$^{13}C$ dipolar couplings. The signals of CH and $CH_2$ groups could thus be suppressed, leaving only the signals of quaternary carbon and methyl group (Harris, 1986).

$^{1}H$ spin-lattice relaxation times in the laboratory frame ($^{1}H$-$T^{1}$) were measured in rotating conditions (10 kHz) with inversion-recovery pulse sequence and recovery times from 10 μs to 40 s. The recycling delay in these experiments was 10 s.

2D $^{1}H$-$^{13}C$ heteronuclear correlation (HETCOR) spectra were recorded following the sequence presented by van Rossum et al. (1997). The pulse sequence starts with a ($\pi/2 + \theta_m$) pulse on protons, where $\theta_m$ is the magic angle, followed by a train of off-resonance frequency-switched Lee–Goldburg (FSLG) pulses, (or flip-flop LG (FFLG)) to cancel

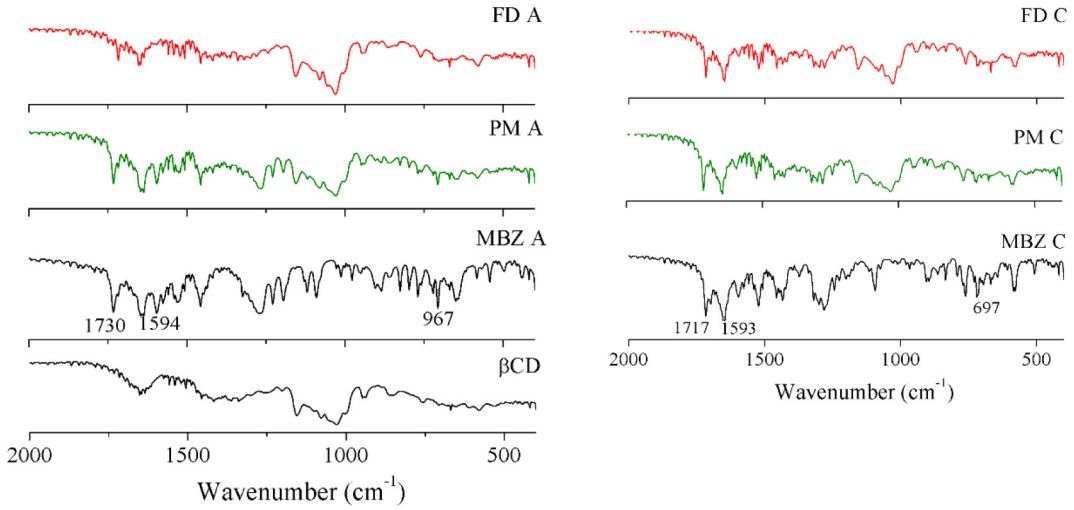


**Fig. 2.** FT-IR spectra of MBZ (polymorphs A and C), β-CD, freeze-dried inclusion complexes (FD) and the corresponding physical mixtures (PM) registered in the 2000–400 $cm^{-1}$ range.

the first two terms of the $^{1}H$–$^{1}H$ dipolar coupling Hamiltonian in the tilted rotating frame. FSLG irradiation was applied during the $t_1$ evolution period in successive times τ, corresponding to a complete 2π rotation around the tilted axis. After the train of FSLG pulses, the proton magnetization was flipped back in the transverse plane by the magic-angle pulse. A ramped-amplitude CP sequence was used to enhance $^{13}C$ signals, and the SPINAL-64 pulse sequence was used to decouple protons during $^{13}C$ signal acquisition. The period τ was set to 7.68 μs. The CP contact time was set to 200 μs, to avoid any relayed homonuclear spin-diffusion-type processes, and the recycle delay was 5 s. The duration of the magic-angle pulse was 2.55 μs. Sixty-four $t_1$ increments with a dwell time of 35.5 μs, corresponding to a total acquisition time of 1.14 ms, were used. The spinning rate was 10 kHz.

### 2.5. PXRD

PXRD diagrams were obtained in a Rigaku D-MAX IIIC (Rigaku Co, Tokio, Japan) diffractometer using Cu Kα radiation (Ni-filter) and NaCl and quartz as external calibration standards. The diffractograms were recorded in the 2θ angle range of 3–50° and the process parameters were set at 0.02° scan step size and 2 s scan step time.

### 2.6. Molecular modelling

The molecular geometries of β-CD, MBZ and the inclusion complexes were fully optimized using the semi-empirical PM3 model (Parametric Model 3) (Stewart, 1989). Initial coordinates of β-CD were obtained from crystallographic data (Sharff et al., 1993). The vibrational frequencies were calculated to confirm that the stationary points were true minima. A previously adopted procedure was followed to simulate the inclusion process (Filippa et al., 2008; Sancho et al., 2015), and two possible orientations were considered: the "Head Up" and "Head Down" orientations, in which MBZ initially points toward the primary and the secondary hydroxyls of β-CD, respectively. A total of 22 structures for each orientation were calculated, in order to ensure that the MBZ passes through the entire β-CD cavity. The PM3 optimized geometries of minimum energy were further optimized using the DFT B3LYP/6-31G(d) level of theory. A topological analysis (QTAIM) was performed on these structures using the Multiwfn software (Lu and Chen, 2012) with a wave function generated at the B3LYP/6-311 + + G(d,p) level of theory, in order to quantify relevant interactions in the inclusion complexes. All of the calculations were performed with GAUSSIAN 09 software packages (Frisch et al., 2009).

### 2.7. Physical stability

Physical stability was monitored by ssNMR, to study possible polymorphic transformations. Solid samples of MBZ (A and C), the FDs and PMs were stored in closed glass vials under accelerated conditions at 40 °C and 75% relative humidity (RH), and subjected to daylight in a stability chamber for 6 months. The samples were monitored at predetermined times, initial time ($t = 0$), one month ($t = 1$), three months ($t = 3$) and six months ($t = 6$).

### 2.8. Solubility studies

The effect of β-CD on the solubility of MBZ A and MBZ C at 25.0 ± 0.1 °C in water was studied. The measurements were performed according to the Higuchi-Connors methodology (Higuchi and Connors, 1965). Excess amounts of MBZ A and C (5 mg) were added in vials containing 10 mL of aqueous solutions with increasing amounts of β-CD. The vials were placed in a water bath at constant temperature (25.0 ± 0.1 °C) and shaken until equilibrium was reached (48 h). The solutions were filtered with nylon filters (0.22 μm) and adequately diluted. MBZ concentrations in the solution phase were measured by means of UV–Vis spectroscopy at 290 nm using a Varian Cary50 spectrophotometer.

Equilibrium solubilities of MBZ (A and C), the FDs (A and C) and the PMs (A and C) samples were measured using the saturation *shake-flask* method at 37 °C, following a known procedure (Sancho et al., 2015). Two different dissolution media were employed: HCl/KCl buffer solution (pH 1.5) and phosphate buffer solution (pH 7.4). The ionic strength of both buffers was fixed at 0.05 M with KCl. All the experiments were carried out in triplicate.

## 3. Results

### 3.1. FT-IR

The FT-IR spectra of MBZ (A and C), β-CD, FD A, FD C, PM A and PM C are shown in Fig. 2. In order to improve the clarity, this figure shows the spectra in the 2000–400 $cm^{-1}$ range and the full spectra of the samples are depicted in supplementary material (Fig. S1). MBZ A and MBZ C exhibited characteristic bands at 1730 and 1717 $cm^{-1}$, respectively (Kumar et al., 2008). These signals could be assigned to stretching vibration of the C=O group (amide band I). Also, the N–H stretching signals located at 3369 $cm^{-1}$ (MBZ A) and 3400 $cm^{-1}$ (MBZ C) could be observed in the registered spectra. Another set of important

bands of both polymorphs are located at 1647 (νC=O, ketone), 1593 (νN=C) and 697 (δN−H) $cm^{-1}$. The FT-IR spectra of FD A and FD C are different from the free polymorphs and the PM samples. The most important changes are associated with the intensity reduction of the bands located at 1593 and 697 $cm^{-1}$, observed in forms A and C, which almost disappeared in the FD A and FD C spectra. In addition, the carbonyl stretching band suffered a small shift upon complexation. These observations are indicative of intermolecular interactions between MBZ and β-CD, suggesting that a new solid phase has been formed. On the other hand, no important changes were observed in the PM spectra, which were the simple superposition of the MBZ and β-CD spectra, for both polymorphs.

### 3.2. ssNMR

Solid state NMR provided a direct way to identify and analyse the polymorphic forms of drugs, and additionally, it was widely applied to probe drug-CD interactions in solid complexes (Chattah et al., 2013; Garnero et al., 2014; Monti et al., 2014).

#### 3.2.1. Characterization of MBZ A and MBZ C by 1D spectra

Fig. 3 (bottom) displays the solid state $^{13}C$ CP-MAS spectra for MBZ A and C. The quaternary carbon edition spectra are shown in Fig. S2 of the Supplementary material. The assignments were made according to NMR data in solution (Al-Badr and Tariq, 1987) and the quaternary and methyl group carbon edition spectra for each polymorph. The resonances were also compared with the reported solid state NMR spectra of albendazole polymorphs. Albendazole is a related compound with similar chemical structure (Chattah et al., 2015). Table 1 lists the $^{13}C$ chemical shifts for the assigned resonances in both polymorphs.

From the spectra and the corresponding chemical shifts, it was possible to clearly identify polymorphs A and C of MBZ, due to changes in almost all of the resonances. Consider for example, C14 that appeared at 50.6 ppm for MBZ A, where in MBZ C its resonance was at 53.6 ppm. Another important notable shifts occurred for C11, that was at 154.8 ppm in MBZ A and at 153.2 ppm in MBZ C, and for C2, which was at 150.2 ppm in MBZ A and 148.4 ppm in MBZ C. Note that, except for the two resonances at around 50 ppm for the methyl group and 200 ppm corresponding to C=O (C15), most of the signals were concentrated in the range 110–160 ppm.

**Table 1**
$^{13}C$ chemical shifts for the assigned resonances in MBZ A and MBZ C.

| Carbons | MBZ A | MBZ C |
|---|---|---|
| | $^{13}C$ chemical shifts (ppm) | |
| 14 | 50.6 | 53.6 |
| 9,8,6 | 116.4, 123.4, 113.3 | 122.7, 120.9, 111.8 |
| 18–22 | 131.6-129.8-126.9 | 134.8-131.4-129.6 |
| 7 | 130.8 | 131.6 |
| 4,17,5 | 141.2-135.4 | 137.2-136.2-132.9 |
| 2 | 150.2 | 148.4 |
| 11 | 154.8 | 153.2 |
| 15 | 194.5 | 196.2 |

#### 3.2.2. Characterization of MBZ A and MBZ C by $^{1}H$-$^{13}C$ correlation spectra

Fig. 4 show the 2D $^{1}H$-$^{13}C$ HETCOR NMR spectra for MBZ A and C, performed at 10 kHz MAS. A short contact time of 200 μs was used during the CP period that allowed for developing short-range heteronuclear correlations only. The carbon spectra were shown in the direct projection (horizontal, F1), while the proton spectra were shown in the indirect dimension (vertical, F2). The 2D spectra displayed well-resolved correlations between carbons and their neighbouring protons. These spectra were useful to complete the carbon assignments and to extract the $^{1}H$ chemical shifts. The first observation was that the correlations and the $^{1}H$ projections were different for both polymorphic forms, revealing particular inter and intra-molecular correlations. Table 2 displays $^{1}H$ chemical shifts obtained from the heteronuclear correlations.

Note that for the aromatic protons, two groups could be recognized,

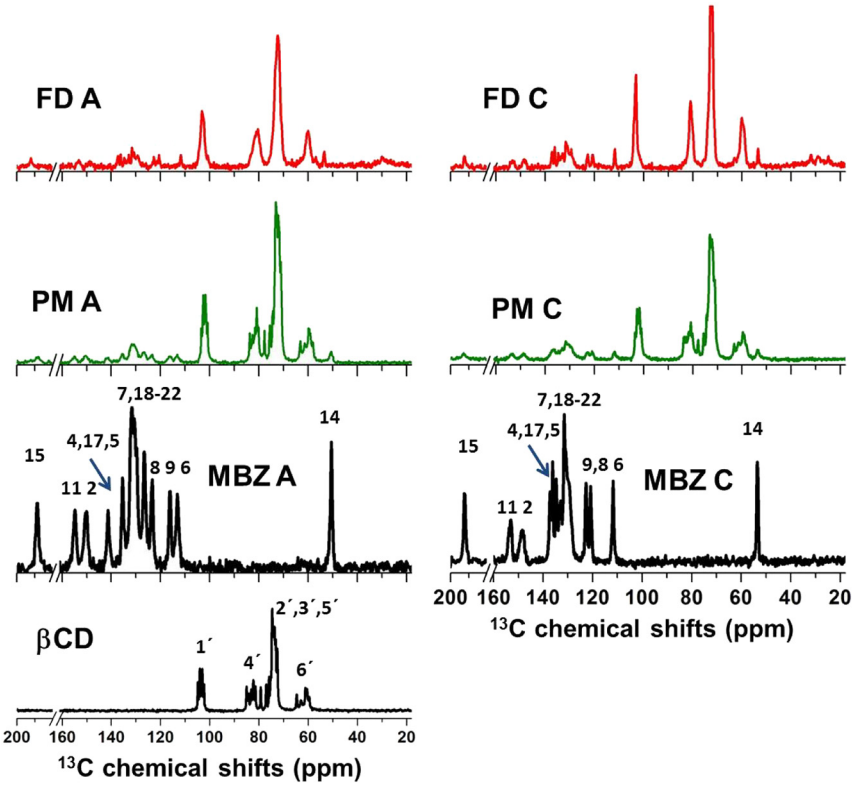


**Fig. 3.** $^{13}C$ CP-MAS spectra of MBZ (polymorphs A and C), β-CD, freeze-dried inclusion complexes (FD) and the corresponding physical mixtures (PM).

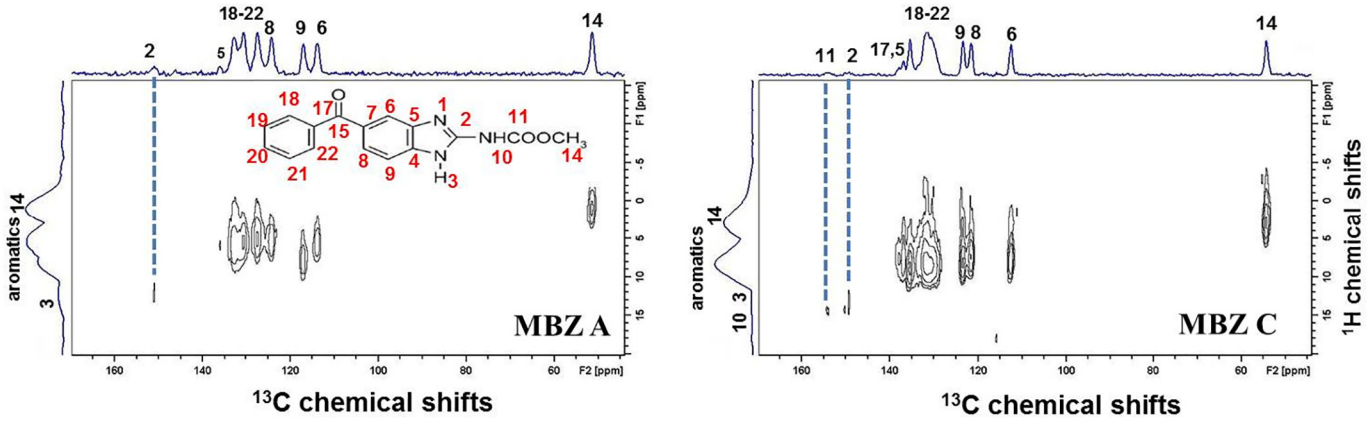


**Fig. 4.** 2D $^{1}$H-$^{13}$C HETCOR spectra of MBZ A and MBZ C. $^{13}$C and $^{1}$H projections are displayed in the direct and indirect frequency dimensions, respectively. Relevant correlations are marked with dashed lines. Assignments are shown for the carbon spectra and some protons.

**Table 2**
$^{1}$H chemical shifts (in ppm) extracted from the correlations in the 2D HETCOR spectra. Errors in chemical shifts are around 0.5 ppm.

| Protons | MBZ A | MBZ C |
|---|---|---|
| | $^{1}$H chemical shifts (ppm) | |
| 14 | 1.0 | 2.8 |
| 9,6,8 | 7.8, 5.6, 5.4 | 8.1, 7.8, 7.4 |
| 18–22 | 4.9-5.2-5.6 | 8.7-8.4-8.2 |
| 3 | 12.3 | 13.3 |
| 10 | – | 14.7 |

belonging to the different aromatic rings in the molecule. In both polymorphs it was possible to observe that quaternary carbons C(4,5,17) also displayed correlations with the nearest aromatic protons.

Quaternary carbons C2 and C11 displayed correlations with protons at higher ppm, that can be assigned to NH protons, H3 and H10. For MBZ C, C2 had noticeable correlations with both protons, where C11 displayed correlations with only one NH proton. In contrast, in MBZ A, only C2-H3 correlation was visible. Besides, in contrast with albendazole, the H1 proton could not be observed. Indeed, not only $^{13}$C spectra but also $^{1}$H spectra could be distinguished in the polymorphs. This was in contrast with the results obtained for the albendazole solid forms I and II, which were classified as desmotropes (Chattah et al., 2015).

### 3.2.3. Characterization of the binary complexes by 1D spectra

Fig. 3 displays the $^{13}$C CP-MAS spectra of the β-CD, FD and PM samples. The $^{13}$C CP-MAS spectrum of βCD showed multiple and sharp resonances for each type of carbon (in the region 50–110 ppm), typical of crystalline systems, and was previously correlated with distinct values of dihedral angles of the glycosidic alfa (1 → 4) bond for carbons 1 and 4, and with torsion angles describing the orientation of the hydroxyl groups (Zoppi et al., 2011; Braga et al., 2003; Gao et al., 2006). It is interesting to note that the carbon signals corresponding to MBZ polymorphs were in a different region of those belonging to β-CD $^{13}$C spectrum.

The $^{13}$C spectra of the PM A and C were mostly the superposition of the separated spectra of the corresponding polymorph (A or C) and the β-CD. This fact gives evidence that mayor interactions do not occur during the mixing of the solids. Indeed, some differences between both PMs could be observed in the zone of the aromatic carbons of MBZ, between 110 and 140 ppm.

The FD A and FD C spectra showed that the signals belonging to β-CD (C1′–C6′) were broadened and formed groups of wide signals in the range 50–110 ppm, displaying less degree of crystallinity than the corresponding PMs. This fact is indicative that the complexes were new solid forms, different from the precursors. Moreover, the presence of MBZ signals with the same chemical shifts as in the free drug spectrum (in the region 110–200 ppm), suggests that a certain amount of pure drug remained, without interaction with β-CD. The presence of pure residues of drugs (MBZ) is something seen frequently in complexes with β-CD, and it has been observed previously with norfloxacin, furosemide (Chattah et al., 2013; Garnero et al., 2014) and albendazole complexes (Chattah et al., 2017).

Although FD A and FD C $^{13}$C spectra were quite similar, there were some differences that could be distinguished, especially in the wide signal at 80 ppm and a group of signals around 30 ppm, that was present in both FD samples, but absent in the PMs.

### 3.2.4. Characterization of the binary complexes by $^{1}$H-$T_1$ relaxation analysis

A further identification of the pure polymorphs and their corresponding complex formation was obtained through $^{1}$H-$T_1$ relaxation-time experiments. To determine the $T_1$ values from the inversion-recovery experiments, the broad $^{1}$H spectrum was integrated to obtain the magnetization as a function of the recovery time. Then, the behaviour of $^{1}$H magnetization was fitted using one or two relaxation times.

On one side, the two polymorphs displayed well differentiated long relaxation times, 6.3 s and 11.4 s for MBZ A and C, respectively, where for β-CD, a relaxation time of 1.0 s was reported (Garnero et al., 2014).

In the case of each PM, two relaxation times could be assigned, the shorter ones with the major proportion of the sample (around 90%) being 1.05 s and 0.95 s for PM A and PM C, respectively. The minor proportion of each sample was associated with long $T_1$ values, of the order of several seconds. The shorter $T_1$ values in the PMs are close to the β-CD value, inside the error interval that was 5% in all the cases. The longer $T_1$ values corresponded to the amount of pure MBZ, as expected in the PMs.

For each FD sample, once again, two relaxation time values could be extracted from the experiments, one short value with the major proportion (more than 93%) and a long value, of the order of several seconds for the minor proportion of the samples. In this case, the shorter $T_1$ values were 0.87 s and 0.73 s for FD A and C, respectively, with an error below 2%. These values were distinct from the β-CD relaxation time, confirming that the complexes were new solid forms, different from the corresponding PMs. In addition, the different $T_1$ values confirm that FD A and FD C are different solid forms. On the other hand, the presence of a minor proportion of sample in each complex displaying a long $T_1$, represented an amount of pure drug remaining after the complexation, as was observed by the $^{13}$C spectra. Nevertheless, the values were not characteristic enough to distinguish which polymorph was present, probably due to the small amount of pure drug in each complex.

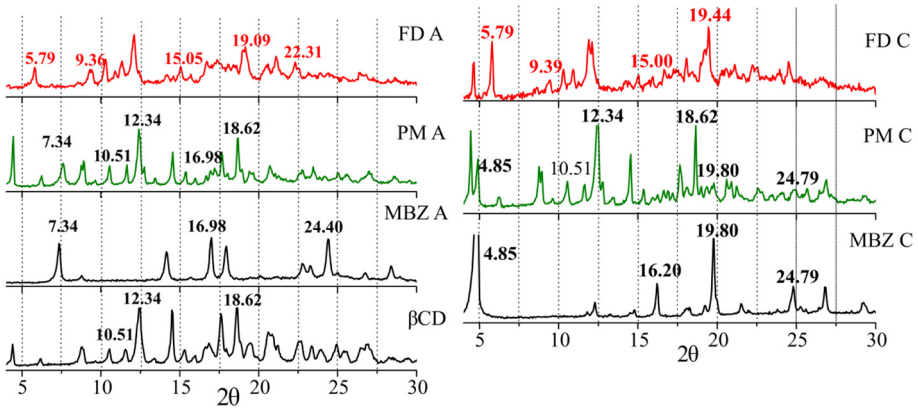


**Fig. 5.** Powder X-ray diffractograms of MBZ (polymorphs A and C), β-CD, freeze-dried inclusion complexes (FD) and the corresponding physical mixtures (PM).

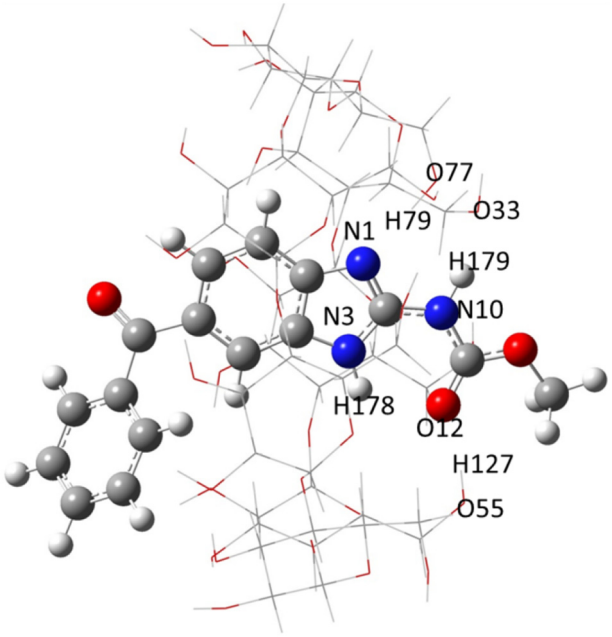


**Fig. 6.** Molecular structure of the MBZ:β-CD inclusion complex in the head down orientation calculated at the B3LYP/6-311 + + G(d,p) level of theory. Hydroxyl groups labelled as O77-H79 and O55-H127 and oxygen labelled as O33 correspond to the β-CD molecule.

### 3.3. PXRD

The diffractograms of MBZ (A and C), β-CD, the PMs (A and C) and the FDs (A and C) samples are illustrated in Fig. 5. The diffraction patterns of MBZ A and MBZ C were consistent with diffractograms reported in the literature for these polymorphs (Brusau et al., 2008). The diffractograms of the FD samples presented different patterns from those of the starting compounds (β-CD and MBZ). A loss on a crystallinity degree of these samples with respect to MBZ and β-CD was observed, possibly due to changes in particle size and shape after recrystallization. In addition, new and sharp diffractions appeared at 2θ 5.79° and 9.36°, indicating that new solid phases were formed. Comparing both complexes, the relative intensities of some peaks differ, as well as the diffraction peak located at 19.09° in FD A was shifted to 19.44° in the FD C complex. These results suggest that the complexes obtained from MBZ A and MBZ C presented different crystalline forms in the solid state.

Previous reports indicated that crystalline inclusion complexes with CDs can adopt one of four possible crystal packing conformations: a channel type motif, a checker board motif, an intermediate motif and a screw-type motif. According to Caira (2001) the PXRD patterns of the CD inclusion exhibited common features for complexes within the same isostructural series. These common features were independent of the nature of the guest molecule included. The observed diffractions for FD A and FD C at 2θ 5.79°, 9.36° and 10.30° are in agreement with the dimeric head-to-head β-CD complex with an intermediate crystal packing structure (Elasaad et al., 2012).

Otherwise, the PM A and PM C presented diffractions patterns similar to MBZ (A and C) and β-CD. The β-CD peaks were not modified, while a lower intensity and a broadening in the characteristic diffraction peaks of MBZ were observed in the PM samples. This result suggests that the crystallinity of MBZ may be altered after the mixture for the sample preparation.

### 3.4. Molecular modelling

The structural and energetic characteristics of the MBZ:β-CD inclusion complex was also investigated using quantum mechanics simulations. The stabilization energy (ΔE) of the inclusion complex formation was calculated with the equation:

$$\Delta E = E_{complex} - (E_{MBZ} + E_{\beta CD}) \quad (1)$$

Two possible orientations were considered for the inclusion process, the head up and the head down orientations. The ΔE values obtained from PM3 calculations were ΔE = −42.1 kJ/mol for the head down orientation, and ΔE = −35.2 kJ/mol for the head up. The stabilization energy calculated with the B3LYP/6-31G(d) level of theory also indicated that the head down orientation was energetically the most stable structure (ΔE = −107.5 kJ/mol for the head down and ΔE = −80.3 kJ/mol for the head up).

The molecular structure of the MBZ:β-CD inclusion complex of minimum energy calculated with the DFT method is illustrated in Fig. 6. It can be observed that the benzimidazole moiety of MBZ is completely embedded in the CD cavity and the rest of the molecule remains outside. In addition, the relative position of the amide group favours the interaction with primary hydroxyls of β-CD. The molecular structure of MBZ suffered some changes when the complex was formed. The most significant one was observed in the dihedral angle between the phenyl rings of the benzophenone part. This angle was shifted by almost 180° in the complexed MBZ, in comparison to the free drug. In addition, the intramolecular H-bond length of MBZ between the NH of the imidazole group and the carbonyl of the amide was slightly reduced; it went from 2.100 Å in the free drug to 2.076 Å in the inclusion complex.

The intermolecular interactions between MBZ and β-CD can be appropriately described using the QTAIM (Bader, 1985). The QTAIM specifies that the presence of a bond critical point (BCP) between any two atoms is indicative of an interaction between them. The nature of

**Table 3**
Bond critical points (in a.u.) of the intermolecular H-bonds interactions calculated for the isolated MBZ and the MBZ:β-CD complex with Bader's theory.

| Critical point | ρ | $\nabla^2\rho$ |
|---|---|---|
| MBZ | | |
| *Intramolecular interactions* | | |
| BCP O12…H178N3 | 0.0213 | 0.0722 |
| RCP O12C11N10C2N3H178 | 0.0137 | 0.0786 |
| MBZ:βCD | | |
| *Intramolecular interactions* | | |
| BCP O12…H178N3 | 0.0225 | 0.0760 |
| RCP O12C11N10C2N3H178 | 0.0138 | 0.0796 |
| *Intermolecular H-bonds* | | |
| BCP N10H179…O33 | 0.0241 | 0.0701 |
| BCP N1…H79O77 | 0.0290 | 0.0688 |
| BCP O12…H127O55 | 0.0272 | 0.0837 |
| BCP N1…H104 | 0.0073 | 0.0258 |

BCP and RCP correspond to bond critical point and ring critical point, respectively.

this interaction can be described with the topological parameters of the BCP, such as the electron density ρ(r) and its Laplacian $\nabla^2\rho$. The ρ(r) values for the intermolecular H-bonds are in the range of 0.002–0.04 a.u. and the corresponding Laplacian values are in the range of 0.024–0.137 a.u. The QTAIM analysis of the MBZ:β-CD complex reveals the presence of 4 intermolecular H-bonds between the guest and the host molecules (Fig. S3 of the Supplementary material). The topological parameters of these interactions are listed in Table 3. We observed that the H-bonds between the imidazolic C═N and the amide C═O of MBZ with OH groups of β-CD were particularly strong. In addition, the ρ(r) and $\nabla^2\rho$ values of the intramolecular H-bond of MBZ were slightly higher in the complex than in the isolated molecule, suggesting that this bond underwent a small reinforcement when the complex was formed.

These interactions serve to increase the stability of the complex (Sancho et al., 2016). It is important to note that these intermolecular H-bonds were in good agreement with the experimental FT-IR spectra of the complexes.

### 3.5. Physical stability

In the stability study, the samples were analysed by ssNMR at the initial time and after one, three and six months ($t = 0$, $t = 1$, $t = 3$, and $t = 6$), to examine possible changes or transformations under accelerated storage conditions. Fig. 7 displays the $^{13}C$ CP-MAS for MBZ (A and C), the FDs (A and C) and the PMs (A and C) samples. In particular, both MBZ A and C spectra displayed no changes at the different studied times, remaining almost identical in chemical shifts and intensities. This fact indicates that both MBZ A and C maintained the same structure under storage conditions, revealing the absence of polymorphic transformations. For the FD samples, it was possible to observe some minor changes over the different storage times, mainly in the intensity of the signals, although there was no appearance of new signals or disappearance of the original signals of the FD A or C spectra at $t = 0$. Therefore, these unchanged spectra, as a function of storage time, are indicative that both FD A and FD C were stable under storage conditions, and that they preserved the characteristics of physical stability of the corresponding pure polymorphs. For both PMs, it was possible to observe the same spectra throughout the 6 months of storage, without changes in shape, intensity or chemical shifts.

### 3.6. Solubility studies

Phase solubility diagrams were built relating the MBZ solubility with the β-CD concentration in aqueous solutions. Following the Higuchi-Connors approximation, the apparent stability constant ($K_C$) and the stoichiometry of the inclusion complex can be derived (Higuchi and Connors, 1965). The solubility diagrams of MBZ A and MBZ C with β-CD are presented in Fig. S4 (Supplementary material). A linear increase in the drug solubility with increasing concentrations of β-CD was observed, suggesting that the MBZ solubility is enhanced through the formation of the inclusion complex. Both systems (MBZ A and MBZ C) can be classified as $A_L$ type (Frömming and Szejtly, 1994), and the $K_C$ values and stoichiometry of the complexes can be derived using the following equation:

$$S_t = S_0 + \frac{K_C S_0 [\beta CD]}{1 + K_C S_0} \quad (2)$$

$S_t$ and $S_0$ are the total and intrinsic MBZ solubility (without β-CD), respectively. Slopes lower than 1 in Eq. (2) are indicative of 1:1 stoichiometry (Connors, 1996). This is the case of the solubility diagrams of MBZ A and MBZ C with β-CD, which means that both inclusion complexes have a 1:1 stoichiometry in aqueous solutions. Moreover, the apparent stability constants are $K_C = 1205\ M^{-1}$(MBZ A) and $K_C = 2001\ M^{-1}$ (MBZ C).

The equilibrium solubility of MBZ (A and C) and the solid samples (FDs and PMs) were measured in two dissolution media at 37 °C and the results are presented in Table 4. The solubilities of MBZ A and C are very low at pH 7.4 (≈2 μg/mL). These values increase at pH 1.5, being MBZ C almost five times more soluble than MBZ A. The FD samples show an important solubility increase of MBZ at acidic pH for both polymorphs (a 5-fold and 2.5-fold increase for MBZ A and C, respectively). At pH 7.4, the MBZ solubility is only affected in the polymorph C, the FD C complex increase it value in almost 4 times. Negligible improves in the drug solubility are observed in the FD A samples at pH 7.4. Finally, the aqueous solubilities of MBZ in the PM samples are very similar to the values measured for the solid free drugs in both dissolution media.

## 4. Conclusions

The polymorphs A and C, of the anthelmintic drug MBZ, were distinguished and fully characterized by 1D spectra and 2D correlation spectra ssNMR. In particular, heteronuclear correlations allowed us to confirm that the forms A and C were truly polymorphs and not desmotropes, as in the previously analysed related compound, albendazole. Is important to note that this study of MBZ in solid state, is the first examination of both polymorphs A and C and their complexes with β-CD by NMR. A complete analysis of the inclusion process of MBZ polymorphs in the cavity of β-CD was investigated in solid state. The experimental characterization employed several techniques (FTIR, PXRD and ssNMR), and revealed evidence of the complexation of both polymorphs with β-CD. Therefore, FD A and FD C, prepared via freeze-dried methodology, constituted new solid forms, different from the corresponding PMs. Although it was difficult to differentiate both solid forms by FT-IR spectroscopy, both PXRD and ssNMR, gave evidence that both complexes could be distinguished. In addition, the $^1H–T_1$ relaxation time measurements provided an additional confirmation of the existence of new distinctive solid forms. On the other hand, the FD diffractograms were comparable with the dimeric head to head β-CD complexes. The molecular modelling analysis indicated that head down is the preferred orientation in the complex and several intermolecular interactions were detected by means of QTAIM. Such interactions are in agreement with the observed changes in the spectroscopic studies. It was interesting to note that our results demonstrated that the complexes maintained the physical stability of the polymorphs, in accelerated storage conditions. Finally, an increase in the aqueous solubility of the drug by FD A and FD C inclusion complexes was determined. Therefore, the new MBZ:β-CD complex constitutes an interesting alternative for the development of MBZ pharmaceutical formulations with improved properties.

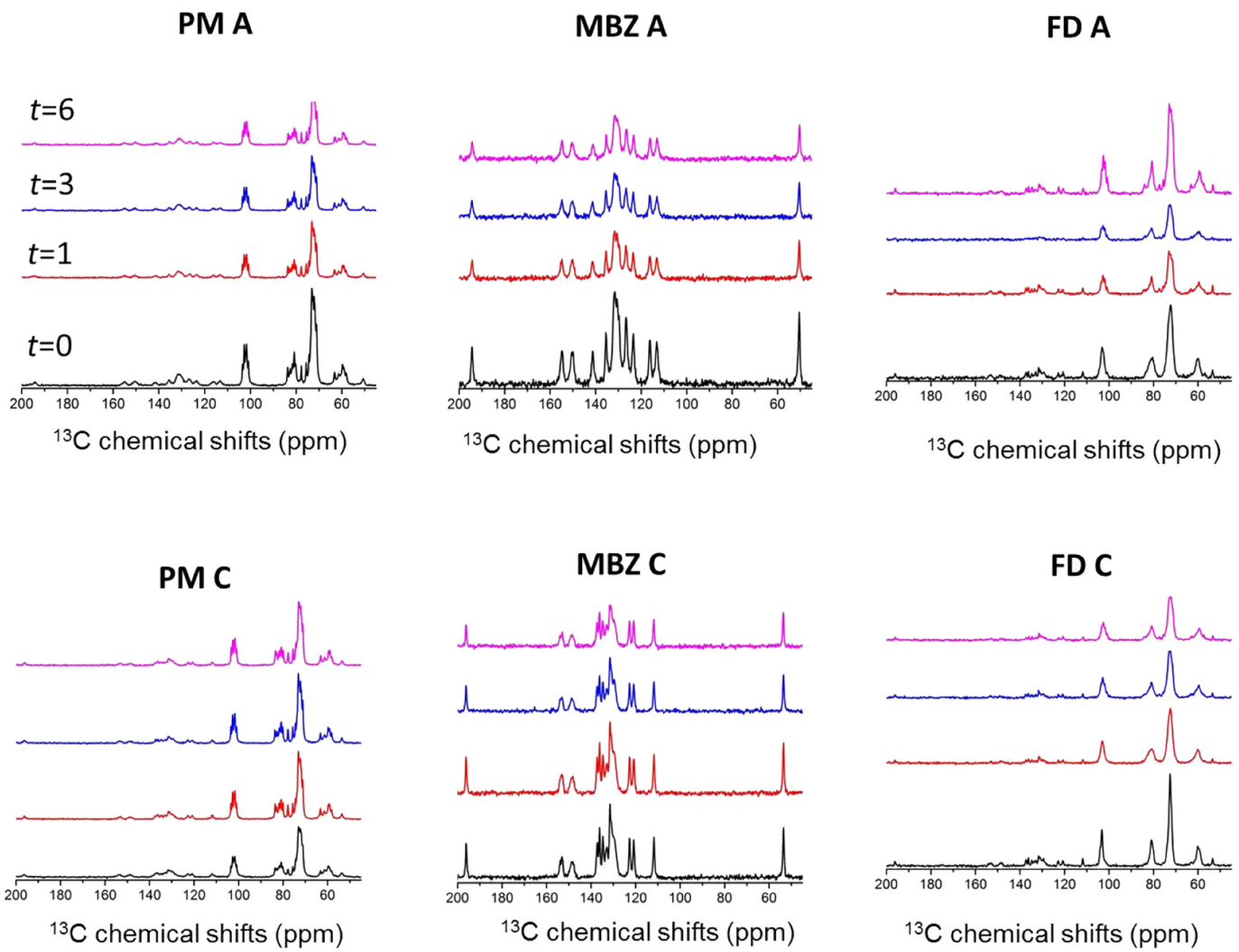


**Fig. 7.** $^{13}$C CP-MAS spectra of MBZ (polymorphs A and C) FD and PM systems at the selected times for the stability study: initial time ($t$ = 0), 1 month ($t$ = 1), 3 months ($t$ = 3), 6 months ($t$ = 6).

**Table 4**
Solubility of MBZ (μg/mL) in different media at 37 °C. Results are reported as the mean of three replicates.

| | pH 1.5 | pH 7.4 |
|---|---|---|
| MBZ A | 13.5 ± 0.9 | 2.1 ± 0.1 |
| MBZ C | 54.2 ± 3.9 | 1.8 ± 0.6 |
| FD A | 69.6 ± 6.6 | 2.4 ± 0.1 |
| FD C | 133.4 ± 3.7 | 8.0 ± 0.5 |
| PM A | 33.2 ± 1.1 | 2.3 ± 0.1 |
| PM C | 52.4 ± 0.7 | 2.0 ± 0.5 |

## Acknowledgments

The authors wish to acknowledge the assistance of the Consejo Nacional de Investigaciones Científicas y Técnicas (CONICET) and the Universidad Nacional de Córdoba, both of which provided support and facilities for this investigation. Also, this work was supported by the Secretaría de Ciencia y Técnica de la Universidad Nacional de Córdoba (SECyT-UNC), Secretaría de Ciencia y Técnica de la Universidad Nacional de San Luis (SECyT-UNSL) and the Fondo para la Investigación Científica y Tecnológica (FONCYT).

## Appendix A. Supplementary data

This material shows the FTIR spectra of MBZ A and C, β-CD, FD and PM samples in the 4000–400 cm$^{-1}$ (Fig. S1), $^{13}$C CP-MAS quaternary carbons and methyl groups spectra for MBZ A and C (Fig. S2), a molecular graph of the MBZ:β-CD inclusion complex obtained with the QTAIM methodology and calculated at the B3LYP/6-311 + + G(d,p) level of theory (Fig. S3) and the phase solubility diagrams of MBZ A and MBZ C with βCD in aqueous solutions at 25 °C (Fig. S4).

## References

Al-Badr, A., Tariq, M., 1987. Analytical profile of mebendazole. In: Analytical Profiles of Drug Substances, pp. 291–326.
Aloisio, C., Longhi, M.R., De Oliveira, A.G., 2015. Development and characterization of a biocompatible soybean oil-based microemulsion for the delivery of poorly water-soluble drugs. J. Pharm. Sci. 104, 3535–3543.
Bader, R., 1985. Atoms in molecules. Acc. Chem. Res. 18, 9–15.
Braga, S., Goncalves, I., Herdtweck, E., Teixeira-Dias, J., 2003. Solid state inclusion compound of S-ibuprofen in beta-cyclodextrin: structure and characterisation. New J. Chem. 27, 597–601.
Brusau, E.V., Camí, G.E., Narda, G.E., Cuffini, S., Ayala, A.P., Ellena, J., 2008. Synthesis and characterization of a new mebendazole salt: mebendazole hydrochloride. J. Pharm. Sci. 97, 542–552.
Caira, M.R., 2001. On the isostructurality of cyclodextrin inclusion complexes and its practical utility. Rev. Roum. Chim. 46, 371–386.
Charoenlarp, P., Waikagul, J., Muennoo, C., Srinophakun, S., Kitayaporn, D., 1993. Efficacy of single-dose mebendazole, polymorphic forms A and C, in the treatment of

hookworm and *Trichuris* infections. Southeast Asian J. Trop. Med. Public Health 24, 712–716.
Chattah, A.K., Mroue, K.H., Pfund, L.Y., Ramamoorthy, A., Longhi, M.R., Garnero, C., 2013. Insights into novel supramolecular complexes of two solids forms of norfloxacin and β-cyclodextrin. J. Pharm. Sci. 102, 3717–3724.
Chattah, A.K., Zhang, R., Mroue, K.H., Pfund, L.Y., Longhi, M.R., Ramamoorthy, A., Garnero, C., 2015. Investigating albendazole desmotropes by solid-state NMR spectroscopy. Mol. Pharm. 12, 731–741.
Chattah, A.K., Pfund, L.Y., Zoppi, A., Longhi, M.R., Garnero, C., 2017. Toward novel antiparasitic formulations: complexes of albendazole desmotropes and β-cyclodextrin. Carbohydr. Polym. 164, 379–385.
Chiba, Y., Kohri, N., Iseki, K., Miyazaki, K., 1991. Improvement of dissolution and bioavailability for mebendazole, an agent for human echinococcosis, by preparing solid dispersion with polyethylene glycol. Chem. Pharm. Bull. 39, 2158–2160.
Connors, K.A., 1996. Measurement of cyclodextrin complex stability constants. In: Szejtli, J., Osa, T. (Eds.), Comprehensive Supramolecular Chemistry. vol. 3 Elsevier, Oxford, UK.
de Melo, P.N., Barbosa, E.G., Garnero, C., de Caland, L.B., Fernandes-Pedrosa, M.F., Longhi, M.R., da Silva-Júnior, A.A., 2016. Interaction pathways of specific co-solvents with hydroxypropyl-β-cyclodextrin inclusion complexes with benznidazole in liquid and solid phase. J. Mol. Liq. 223, 350–359.
De Oliveira, M.G., Guimarães, A.G., Araújo, A.A., Quintans, J.S., Santos, M.R., Quintans-Júnior, L.J., 2015. Cyclodextrins: improving the therapeutic response of analgesic drugs: a patent review. Expert Opin. Ther. Pat. 25, 897–907.
Elasaad, K., Alkhatib, R., Hennebelle, T., Norberg, B., Wouters, J., 2012. Determination of the absolute configuration of aegelinol by crystallization of its inclusion complex with β-cyclodextrin. Crystals 2, 1441–1454.
Filippa, M., Sancho, M.I., Gasull, E., 2008. Encapsulation of methyl and ethyl salicylates by β-cyclodextrin. HPLC, UV–vis and molecular modeling studies. J. Pharm. Biomed. Anal. 48, 969–973.
Frisch, M.J., Trucks, G.W., Schlegel, H.B., Scuseria, G.E., Robb, M.A., Cheeseman, J.R., Scalmani, G., Barone, V., Mennucci, B., Petersson, G.A., et al., 2009. Gaussian09 Revision D.01. Gaussian Inc., Wallingford CT.
Frömming, K.H., Szejtly, J., 1994. Cyclodextrins in Pharmacy. Kluwer Academic Publishers, Dordrecht, the Netherlands.
Fung, B.M., Khitrin, A.K., Ermolaev, K., 2000. An improved broadband decoupling sequence for liquid crystals and solids. J. Magn. Reson. 142, 97–101.
Gao, Y., Zhao, X., Dong, B., Zheng, L., Li, N., Zhang, S., 2006. Inclusion complexes of β-cyclodextrin with liquid surfactants. J. Phys. Chem. B 110, 8576–8581.
Garnero, C., Zoppi, A., Genovese, D., Longhi, M., 2010. Studies on trimethoprim:hydroxypropyl-β-cyclodextrin: aggregate and complex formation. Carbohydr. Res. 345, 2550–2556.
Garnero, C., Aiassa, V., Longhi, M., 2012. Sulfamethoxazole:hydroxypropyl-β-cyclodextrin complex: preparation and characterization. J. Pharm. Biomed. Anal. 63, 74–79.
Garnero, C., Chattah, A.K., Longhi, M., 2014. Improving furosemide polymorphs properties throughsupramolecular complexes of β-cyclodextrin. J. Pharm. Biomed. Anal. 95, 139–145.
Gottstein, B., Stojkovic, M., Vuitton, D.A., Millon, L., Marcinkute, A., Deplazes, P., 2016. Threat of alveolar echinococcosis to public health - a challenge for Europe. Trends Parasitol. 31, 407–412.
Harris, R.K., 1986. Nuclear Magnetic Resonance Spectroscopy: A Physicochemical View. Longman Scientific & Technical, Essex, U.K.
Higuchi, T., Connors, K.A., 1965. Phase solubility techniques. Adv. Anal. Chem. Instrum. 4, 117–212.
Hollingsworth, T.D., Adams, E.R., Anderson, R.M., Atkins, K., Bartsch, S., Basáñez, M.-G., Behrend, M., Blok, D.J., Chapman, L.A.C., Coffeng, L., Courtenay, O., Crump, R.E., De Vlas, S.J., Dobson, A., Dyson, L., Farkas, H., Galvani, A.P., Gambhir, M., Gurarie, D., Irvine, M.A., Jervis, S., Keeling, M.J., Kelly-Hope, L., King, C., Lee, B.Y., Le Rutte, E.A., Lietman, T.M., Ndeffo-Mbah, M., Medley, G.F., Michael, E., Pandey, A., Peterson, J.K., Pinsent, A., Porco, T.C., Richardus, J.H., Reimer, L., Rock, K.S., Singh, B.K., Stolk, W., Swaminathan, S., Torr, S.J., Townsend, J., Truscott, J., Walker, M., Zoueva, A., 2015. Quantitative analyses and modelling to support achievement of the 2020 goals for nine neglected tropical diseases: where are we now? Parasit. Vectors 8 (art. no. 630).
Jeang, C.-L., Lin, D.-G., Hsieh, S.-H., 2005. Characterization of cyclodextrin glycosyltransferase of the same gene expressed from *Bacillus macerans*, *Bacillus subtilis*, and *Escherichia coli*. J. Agric. Food Chem. 53, 6301–6304.
Kumar, S., Chawla, G., Sobhia, M.E., Bansal, A.K., 2008. Characterization of solid-state forms of mebendazole. Pharmazie 63, 136–143.
Lu, T., Chen, F., 2012. Multiwfn: a multifunctional wavefunction analyzer. J. Comput. Chem. 33, 580–592.
Martinez-Marcos, L., Lamprou, D.A., McBurney, R.T., Halbert, G.W., 2016. A novel hot-melt extrusion formulation of albendazole for increasing dissolution properties. Int. J. Pharm. 499, 175–185.
Meinguet, C., Masereel, B., Wouters, J., 2015. Preparation and characterization of a new harmine-based antiproliferative compound in complex with cyclodextrin: increasing solubility while maintaining biological activity. Eur. J. Pharm. Sci. 77, 135–140.
Mendes, C., Buttchevitz, A., Kruger, J.H., Kratz, J.M., Simões, C.M.O., De Oliveira Benedet, P., Oliveira, P.R., Silva, M.A.S., 2016. Inclusion complexes of hydrochlorothiazide and β-cyclodextrin: physicochemical characteristics, in vitro and in vivo studies. Eur. J. Pharm. Sci. 83, 71–78.
Metz, G., Wu, X.L., Smith, S.O., 1994. Ramped-amplitude cross polarization in magic-angle-spinning NMR. J. Magn. Reson. Ser. A 110, 219–227.
Monti, G.A., Chattah, A.K., Garro Linck, Y., 2014. Solid-state nuclear magnetic resonance in pharmaceutical compounds. Annu. Rep. NMR Spectrosc. 83, 221–269.
Montresor, A., Stoltzfus, R.J., Albonico, M., Tielsch, J.M., Rice, A.L., 2002. Is the exclusion of children under 24 months from anthelmintic treatment justifiable? Trans. R. Soc. Trop. Med. Hyg. 96, 197–199.
Montresor, A., Awashti, S., Crompton, D.W.T., 2003. Use of benzimidazoles in children younger than 24 months for the treatment of soli-transmitted helminthiasis. Acta Trop. 86, 223–232.
Pinto, L.C., Soares, B.M., Pinheiro, J.D.J.V., Riggins, G.J., Assumpção, P.P., Burbano, R.M.R., Montenegro, R.C., 2015. The anthelmintic drug mebendazole inhibits growth, migration and invasion in gastric cancer cell model. Toxicol. in Vitro 29, 2038–2044.
Sancho, M.I., Russo, M.G., Moreno, M.S., Gasull, E., Blanco, S.E., Narda, G.E., 2015. Physicochemical characterization of 2-hydroxybenzophenone with β-cyclodextrin in solution and solid state. J. Phys. Chem. B 119, 5918–5925.
Sancho, M.I., Andujar, S., Porasso, R.D., Enriz, R.D., 2016. Theoretical and experimental study of inclusion complexes of β-cyclodextrins with chalcone and 2′,4′-dihydroxychalcone. J. Phys. Chem. B 120, 3000–3011.
Sharff, A.J., Rodseth, L.E., Quiocho, F.A., 1993. Refined 1.8-Å structure reveals the mode of binding of β-cyclodextrin to the maltodextrin binding protein. Biochemistry 32, 10553–10559.
Stewart, J.J.P., 1989. Optimization of parameters for semiempirical methods. I. Method. J. Comput. Chem. 10, 209–220.
Surov, A.O., Manin, A.N., Voronin, A.P., Drozd, K.V., Simagina, A.A., Churakov, A.V., Perlovich, G.L., 2015. Pharmaceutical salts of ciprofloxacin with dicarboxylic acids. Eur. J. Pharm. Sci. 77, 112–121.
Swanepoel, E., Liebenberg, W., Devarakonda, B., De Villiers, M.M., 2003. Developing a discriminating dissolution test for three mebendazole polymorphs based on solubility differences. Pharmazie 58, 117–121.
U.S. Pharmacopeia and the National Formulary, 2008. USP30-NF25, United States Pharmacopeia.
van Rossum, B.J., Förster, H., de Groot, H.J.M., 1997. High-field and high-speed CP-MAS $^{13}C$ NMR heteronuclear dipolar-correlation spectroscopy of solids with frequency-switched Lee–Goldburg homonuclear decoupling. J. Magn. Reson. 124, 516–519.
Zoppi, A., Garnero, C., Linck, Y.G., Chattah, A.K., Monti, G.A., Longhi, M.R., 2011. Enalapril:β-CD complex: stability enhancement in solid state. Carbohydr. Polym. 86, 716–721.